

**VOLUME ESTIMATION OF CURVED SURFACES USING
STRUCTURED LIGHTING AND THEIR SIMILARITY MEASURE**

by

AHMED MOHAMED ABD ELMAGID ELNAGGAR

**Thesis submitted in fulfilment of the
requirements for the degree
of Master of Science**

JULY 2006

ACKNOWLEDGEMENTS

I would like to thank *Allah*. He guided and helped me throughout my research.

I have a great appreciation for my supervisor, Associate Professor Dr. Mani Maran a/l Ratnam. Firstly, he gave me the chance to study and explore 3-D measurement. Secondly, he taught me how to be systematic and to how write and express my work. I find what he taught me is what an engineer needs to stand on a solid ground. I would not hesitate to teach and guide people around me by the same way.

I would like to mention my deep respect to my parents. They are extraordinary persons that always inspire me and surround me by their love and care. Today, I really realize that my father is my hero. My father and my mother always teach me how to be honest and patient. I would like to thank my younger sister and brother to keep me smiling all the time. I deeply thank my wife for her support and her patience during my study. She made my study easier and helped me to concentrate.

It was my pleasure to study in Universiti Sains Malaysia. I had met many people that I discussed with them many topics in many areas. My knowledge has significantly increased by these discussions.

I had the chance to meet and make new friendships during my study. I would like to thank Soo Say Leong for the long discussions that improved my knowledge in many areas. I also thank all Arabian friends that made me feel that I am still at home.

Finally, I would like to thank my supervisor for offering me a financial support for a certain period of time.

ACKNOWLEDGEMENTS	ii
TABLE OF CONTENTS	iii
LIST OF TABLES	vi
LIST OF FIGURES	viii
LIST OF ABBREVIATIONS	xii
LIST OF PUBLICATIONS	xiii
ABSTRAK	xiv
ABSTRACT	xvi
CHAPTER ONE : INTRODUCTION	
1.1 Introduction	1
1.2 Research Problem	2
1.3 Research Objectives	2
1.3 Thesis Organization	3
CHAPTER TWO : LITERATURE REVIEW	5
2.1 Introduction	5
2.2 Volume Determination using Non-contact Devices	6
2.3 Segmentation Methods	8
2.4 Shape similarity	13
2.4.1 Feature-Based Method	14
2.4.1.1 Statistical Approach	15
2.4.1.2 Moments	16
2.4.1.3 Geometric Parameters	16
2.4.2 Histogram-Based Method	17
2.4.3 Topology-Based Method	18
2.5 Summary	19
CHAPTER THREE : A SIMULATION STUDY ON THE EFFECT OF FRINGE SPACING ON DIFFERENT VOLUME CALCULATION METHODS IN STRUCTURED LIGHTING	20
3.1 Introduction	20

3.2	Volume Calculation	21
3.2.1	Volume Determination using Multiplication of Area of Base by Height Method	22
3.2.2	Volume Determination using Curve Fitting	24
3.2.2.1	Least Square Polynomial	25
3.2.2.2	Cubic Spline	28
3.3	Proposed Simulation Study	30
3.4	Results	35
3.4.1	Surface Generated using Equation (3.20)	35
3.4.2	Surface Generated using Equation (3.21)	39
3.4.3	Surface Generated using Equation (3.22)	45
3.5	Discussion	47
3.6	Summary	53
 CHAPTER FOUR : DEVELOPMENT OF FRINGE PROJECTION SYSTEM		 55
4.1	Introduction	55
4.2	Design and Development of the Projector	57
4.3	Camera	60
4.3.1	Scaling Factor	61
4.4	Fringe Projection Angle	64
4.5	Summary	66
 CHAPTER FIVE : SYSTEM VALIDATION AND VOLUME MEASUREMENT OF CAPS		 68
5.1	Introduction	68
5.2.	Groundwork	69
5.3	Experimental Procedure	73
5.3.1	The proposed Segmentation Method	73
5.4	Results	75
5.4.1	Spherical cap profile measurement	76
5.4.2	Segmentation	78
5.4.3	Volume Values	78
5.4.4	Root Mean Square Error (RMSE)	79
5.4.5	Point Cloud Data Comparison	80

5.4.6 Area under the Fitted Curve	84
5.5 Discussion	85
5.5.1 Influence of Error in Height on Calculated Volume	86
5.4.2 Limitations of the System	87
5.6 Modelling the Measured Surface	90
5.7 Summary	93
CHAPTER SIX : SHAPE SIMILARITY MEASURE USING GEOMETRIC PARAMETERS	95
6.1 Introduction	95
6.2 Overview of the Approach	96
6.2.1 Determining the Model Principal Axes	99
6.2.2 Bringing the Model into its Canonical Position	101
6.3 Results	102
6.4 Discussion	107
6.5 Summary	114
CHAPTER SEVEN : CONCLUSION AND FUTURE WORK	115
7.1 Conclusion	115
7.2 Future Work	117
REFERENCES	118
APPENDICES	122

LIST OF TABLES

		Page
Table 3.1	Calculated volume of the region under the surface generated using equation (3.20)	36
Table 3.2	Percentage error in calculated volume of the region under the surface generated using equation (3.20)	37
Table 3.3	Calculated volume of the region under the surface generated using equation (3.21)	39
Table 3.4	Percentage error in calculated volume of the region under the surface generated using equation (3.21)	39
Table 3.5	Calculated volume of the region under the surface generated using equation (3.21) at different locations of the grating of line spacing nine	43
Table 3.6	Percentage error in calculated of the region under the surface generated using equation (3.21) at different location of the grating of line spacing nine units	44
Table 3.7	Calculated volume of the region under the surface generated using equation (3.22)	46
Table 3.8	Percentage error of calculated volume of the region under the surface generated using equation (3.22)	46
Table 3.9	Standing of errors in volume and area under the surface generated using equation (3.20).	48
Table 3.10	Error in area of integrating the fitted cubic spline	51
Table 5.1	Cap dimensions and its volume	71
Table 5.2	Error in height of measured surface points	76
Table 5.3	Calculated volume of each spherical cap	78
Table 5.4	Error of calculated volume	79
Table 5.5	Root mean square of all measured surfaces	80
Table 5.6	Percentage error in calculated volume of actual caps using the area of base times its height	86
Table 5.7	Percentage error of calculated volume of measured caps using the area of base times its height	87
Table 5.8	Values of the minimum detected height and their corresponding scaling factor	90

Table 6.1	Classification of spherical caps	96
Table 6.2	Dimensions of scanned models	103
Table 6.3	Values of scale dependency descriptor of the measured spherical caps	104
Table 6.4	Values of scale independency descriptor of the measured spherical caps	105
Table 6.5	Distance matrix of the first 18 scale dependency descriptors	106
Table 6.6	Distance matrix of the first 18 scale independency descriptors	106
Table 6.7	Values of scale dependency descriptor of the actual spherical caps	107
Table 6.8	Values of scale independency descriptor of the actual six spherical caps.	107
Table 6.9	Triangles data of each actual spherical cap	108
Table 6.10	Distance matrix of the six spherical cap scale independency descriptors	109
Table 6.11	Distance matrix of the six spherical cap scale dependency descriptors	112
Table 6.12	Similarity measure between the dependency descriptors of actual spherical caps and their scanned caps	112
Table 6.13	Similarity measure between the independency descriptors of actual spherical caps and their scanned caps	113
Table 6.14	Comparison of descriptors	113

LIST OF FIGURES

		Page
Figure 2.1	Known surface points of a flat object	10
Figure 2.2	Example of a triangulated mesh of known surface points of a flat object	11
Figure 2.3	Schematic of point normal calculation of the method proposed by H. Woo et al. (2002)	13
Figure 2.4	Element-by-element similarity measure	17
Figure 3.1	Structured lighting principles	21
Figure 3.2	Sketch of the captured image for the scanned object in Figure 3.1	21
Figure 3.3	Schematic of volume calculation using area of base times height	23
Figure 3.2	The division of area under the measured surface profile	23
Figure 3.2	Top view of the created rectangles	23
Figure 3.4	Plan and front view for known surface points	24
Figure 3.5	Cubic spline interpolant	29
Figure 3.6	Mesh representation of the generated surface using equation (3.20)	31
Figure 3.7	Mesh representation of the generated surface using equation (3.21)	32
Figure 3.8	Mesh representation of the generated surface using equation (3.22)	32
Figure 3.9	Schematic to calculate the projected point on the surface	34
Figure 3.10	Simulated image for projected lines on the surface generated by equation (3.20) with spacing equals to 4 units	34
Figure 3.11	Volume of the region under the generated surface from equation (3.20)	35
Figure 3.12	Error in calculated volume at different line spacing for the surface generated using equation (3.20)	37

Figure 3.13	Actual profile and interpolated profile using least square polynomial order seven at $x= 62$ of the surface generated using equation (3.20)	38
Figure 3.14	Actual profile and interpolated profile using least square polynomial order nine at $x= 25$ of the surface generated using equation (3.20)	38
Figure 3.15	Error in calculated volume at different line spacing for the surface generated using equation (3.21)	40
Figure 3.16	The location of projected grating with line spacing nine units on the surface generated using equation (3.21)	41
Figure 3.17	Actual profile and interpolated profile using least square polynomial order nine of the surface generated using equation (3.20)	42
Figure 3.18	Percentage error in calculated volume of the region below the surface generated using equation (3.21) at different locations of the grating of line spacing nine units.	44
Figure 3.19	Percentage error in volume of the region below the surface generated using equation (3.21) at different locations of the grating of line spacing four units.	45
Figure 3.20	Error in volume of the region under the surface generated using equation (3.22) at different line spacing	45
Figure 3.21	Actual profile and interpolated profile using cubic spline and least square polynomial order four at $x= 5$ of the surface generated using equation (3.20)	48
Figure 3.22	Location of the x-section on the projected surface	51
Figure 3.23	Spline fitting at different line spacing	52
Figure 3.24	Curve fitted for known coordinate points at angle 20° and 45°	53
Figure 4.1	Schematic diagram of the structured lighting technique used in the experiment	56
Figure 4.2	Collimated and non-collimated light projection over a block	56
Figure 4.3	The experiment setup used in this research	57
Figure 4.4	Sketch of the lens order inside the projector	58
Figure 4.5	The developed projector used in this research	59

Figure 4.6	Fringe pattern	60
Figure 4.7	Image shows the grid after canny edge detection	62
Figure 4.8	Scaling factor values	63
Figure 4.9	Difference between the actual and the average scaling factor for each axis	64
Figure 4.10	Projected fringes on the glass and flat background	65
Figure 4.11	Height value by the lowest, highest and average projection angle	66
Figure 5.1	Cloud data of a spherical cap placed on a flat background	69
Figure 5.2	Mould of six spherical caps	70
Figure 5.3	A Sphere and its cap	70
Figure 5.4	Six moulded caps on a flat background	71
Figure 5.5	Image of the projected pattern on the spherical cap	73
Figure 5.6	Triangulated mesh of the cloud data	75
Figure 5.7	Profile of the measured and the actual cap profile at $y = 200$ pixel	76
Figure 5.8	Profile of the measured and the actual cap profile at $y = 250$ pixel	77
Figure 5.9	Profile of the measured and the actual cap profile at $y = 300$ pixel	77
Figure 5.10	Actual volume and its correspondent measured range	79
Figure 5.11	The standard spherical cap	81
Figure 5.12	The measured spherical cap surface	82
Figure 5.13	Profile of the actual and measured surface at $y=264$ pixel	83
Figure 5.14	Position of the extra known height values	83
Figure 5.15	Area at different y -section	85
Figure 5.16	A zoomed view of several fringes' centres over the cap	88

Figure 5.17	Snapshot of the STL file of cap surface no. 3 on its first measurement	92
Figure 5.18	Top view of the data points	93
Figure 5.19	Snapshot of STL file of the third spherical cap opened on Insight software	93
Figure 6.1	Approach of the proposed method	97
Figure 6.2	The 3D surface with its bounding box	98
Figure 6.3	Cord angle for North and South group for a specific axis	100
Figure 6.4	The 3D model of cap no. 1	102
Figure 6.5	Bounding box at the canonical position	109
Figure 6.6	Triangles area histogram of spherical cap	110

LIST OF ABBREVIATIONS

- CAD : Computer Aided Design
- IGES : Initial Graphics Exchange Specification
- STL : Stereo Lithography
- VRML : Virtual Reality Machine Language

LIST OF PUBLICATIONS

A. M. Elnaggar and M. M. Maran (2005) Determination of volume of smooth surfaces using structured lighting. 9th International on Mechatronics Technology (ICMT'05). 5-8 December 05. Kuala Lumpur – Malaysia.

A. M. Elnaggar and M. M. Maran (2004) Effect of fringe spacing on volume calculation methods in structured lighting: a simulation study. 9th International Conference on computer Graphics, Imaging and Visualization (CGIV'04), 26-29 July 04. Penang – Malaysia.

A. M. Elnaggar and M. M. Maran (2004) Effect of fringe spacing on volume calculation. Proceedings of the Mechanical Engineering Research Colloquium (MERC'04). 7-9 April 04.

PENENTUAN ISIPADU PERMUKAAN-PERMUKAAN LICIN DENGAN
MENGUNAKAN KAEDAH PENCAHAYAAN BERSTRUKTUR DAN
PENGUKURAN KESAMAANNYA

ABSTRAK

Tesis ini membentangkan hasil penyiasatan kaedah tak menyentuh yang dipanggil pencahayaan berstruktur untuk menentukan isipadu permukaan-permukaan licin. Kaedah ini menggunakan kamera yang merakam corak cahaya terubah bentuk yang diunjurkan ke atas suatu permukaan. Sistem tersebut disahkan dengan menggunakan objek-objek yang mempunyai permukaan licin. Pada awalnya, suatu kajian simulasi telah dijalankan untuk menentukan suatu kaedah yang sesuai untuk menentukan isipadu. Suatu kaedah yang sesuai ialah dengan pengamiran lengkung yang dipadan merintangti titik-titik koordinat dan mendarabkan dengan kedalaman sepanjang arah-x. Kesan pic pinggir yang berbeza ke atas isipadu telah dikaji. Kemudian, suatu eksperimen telah dijalankan untuk menentukan isipadu enam tukup sfera. Suatu projektor telah dibina untuk mengunjurkan corak pinggir terkolimat. Sebuah kamera digital telah dikalibrasi untuk menukarkan nilai-nilai piksel kepada milimeter. Ralat dalam 26 pengukuran didapati kurang daripada 8.52%. Suatu kaedah peruasan telah dibangunkan untuk menyari permukaan daripada latarbelakang. Kaedah peruasan tersebut terdiri daripada tiga langkah: (i) jejaring segitiga dijana untuk titik-titik permukaan yang diketahui, (ii) luas setiap segitiga dikira dan (iii) sisihan piawai luas-luas segitiga sekeliling setiap titik permukaan dikira. Semua titik permukaan yang mempunyai sisihan piawai yang sama diruaskan kepada satu kumpulan. Pada akhirnya, kesamaan bentuk antara bentuk-bentuk 3-dimensi dikira. Setiap model 3-D dibawa kepada kedudukan 'canonical' untuk memastikan invarians dalam putaran dan translasi. Pada kedudukan ini, suatu set ciri disari daripada model 3-D tersebut. Jarak kesamaan antara ciri-ciri tersebut dikira dengan menggunakan fungsi *Minkowsky*. Ciri-ciri yang digunakan menunjukkan keputusan yang lebih baik dalam pengukuran kesamaan apabila digunakan pada bentuk yang mempunyai

keunggulan dari garis pusat yang kecil berbanding dengan bentuk yang lebih besar.

Hasil penyelidikan ini boleh digunakan untuk membangunkan suatu sistem tak invasif untuk mengukur tumor kulit.

ABSTRACT

This thesis presents the investigation of a non-contact method called structured lighting to determine volumes of smooth surfaces. This method uses a camera that captures a deformed pattern of light projected upon a surface. The system was verified using objects having a smooth surface. Firstly, a simulation study was carried out to determine a suitable method to determine the volume. A suitable method was found by integration of a fitted curve across coordinate points and multiplied by its depth along x-direction. The effect of different fringe pitches on volume calculation was studied. Secondly, an experiment was carried out to determine the volume of six different spherical caps. A projector was developed to project a collimated fringe pattern. A digital camera was calibrated to convert the pixel values into millimetres. The error in volume of 26 measurements was found to be less than 8.52%. A segmentation method was developed to extract the surface from the background. The segmentation method consists of three steps: (i) a triangular mesh is generated for the known surface points, (ii) the area of each triangle is calculated and (iii) the standard deviation of triangle areas that surround each surface point is calculated. All surface points that have similar standard deviation value are segmented into one patch. Finally, the shape similarity among the measured 3-D shape is calculated. Each 3-D model was brought into its canonical position to ensure its rotation and translation invariance. At this position, a set of features is extracted from the 3-D model and the similarity between all models are measured. This set of features is the cord length of the bounding box. The new features show better accuracy (43.75%) in similarity measure when applied to shapes with smaller height and diameter as compared to the slightly larger shapes. The work of this thesis can be used to develop a non-invasive system to measure skin tumours.

1.1 Overview

Human skin is an organ that protects human muscles and other organs. The skin is responsible for many vital functions. It regulates the body temperature by evaporating water, shields the organism from the environment, protect muscles, produces vitamin D and sensation. The skin is subjected to constant attack such as skin cancer, acnes, tumours, etc. causing pain, malfunction or death in some cases. For example, the tumour malignant melanoma (skin cancer) is affecting 10-12 per 100,000 persons in Europe, 18-20 per 100,000 in the USA and 30-40 per 100,000 in Australia (Schmid-Saugeon et al. 2003). Several medications and treatment strategies were used to heal this ailment. Due to the varieties of existing medications, clinicians measure the volume and area of tumours to investigate the effect of the medication. Schmid-Saugeon et al. (2003) stated the measurement purposes as follows: (i) To document progress of an individual tumour as part of treatment and assessments, (ii) to assess the efficacy of a therapy, (iii) to predict healing time and (iv) to create a database of different disorders or tumours.

The volume and area of skin tumours were previously measured using contact and non-contact methods. A sequence of such measurements allows changes in the shape and volume over a given time period to be monitored. Contact methods were used in a relevant application of measuring the volume of female breasts and wounds. The contact methods for wound measurement used plastic templates, simple ruler or Kundin measuring tool (Krouskop et al. 2002). The disadvantages of contact methods are: (i) they are painful for the patient, (ii) high risk for additional infection and (iii) there is a potential for disrupting the skin tissue when contact is made. On the other hand, non-contact systems overcome these problems with precise measurements. Non-contact systems were used to measure tumour volumes and were applied in other

medical applications. For example, Yeras et al. (2003) used moire topography in the diagnosis of corporal asymmetries. Lilley et al. (2000) used Fourier fringe analysis to measure the human body shape and position during the delivery of radiotherapy treatment for cancer.

1.2 Problem statement

This thesis is primarily concerned with a non-contact measurement called structured lighting method for determining tumour volumes. A pattern of fringe is projected onto a surface to generate the height information on the surface. The extraction of this information is called fringe analysis. The volume of smooth surface can be estimated using the known height information. These surfaces were used to simulate tumours and the problem is to calculate the volume of shapes using this height information.

1.3 Research Objectives

Nowadays, manufacturers need to ensure that their products comply with their specifications to be successful as manufacturing technology improves. A verification process is essential for the system before commercial use to ensure the system complies with the specifications. This verification is performed on known surfaces that have defined volumes. Also, the advance in computer industry creates new areas to be explored and offers new tools to help clinicians. The primary objective of this research is to develop and calibrate a non-contact optical measurement system, which can measure the volume of smooth surfaces. These surfaces were chosen smooth to simulate the 3-D human skin tumours.

The specific objectives of this research can be summarized as:

- i. To identify a suitable method to calculate the volume.

- ii. To investigate the effect of different sizes of pattern of fringes on volume calculation.
- iii. To design, fabricate and assemble a low-cost instrument to project the fringe pattern onto a surface.
- iv. To use the fringe projection system to measure the volume of spherical caps, so that the system calibration and validation are performed.
- v. To develop a new segmentation method based on the triangulated mesh to extract surfaces from the background.
- vi. To determine the shape similarity among 3-D models in the database. This similarity measurement adds a new facility to help clinicians to compare new tumours to the previously measured tumour. An algorithm is applied to measure the similarity between different shapes. This step is necessary to identify the suitable medication if a record is kept for the similar tumours in the database.

The developed non-contact method is subjected to the following constraints:

1. Work in ambient light conditions (clinic or hospital)
2. Able to calculate the volume using one image.

The output of this work can be applied to other applications and is not limited to tumour volume measurement. For example, it can be applied in reverse engineering area, where a CAD file is created from an existing physical part or it can be used for retrieval from a database of 3-D CAD model.

1.4 Thesis Organization

Chapter one introduces the importance of measuring different human skin ailments and the problem of calculating the volume using structured lighting. The details of the

research aims are given. Chapter two reviews the work published in tumour volume measurement and two other relevant areas: wounds and female breasts volume measurement. A review on different segmentation methods is also presented. An introduction for shape similarity and a review of the literature in this area are also presented. A simulation study was carried out within chapter three. A suitable method to calculate the volume is identified among other possible methods. The effect of fringe spacing on volume calculation was investigated and presented in this chapter. Chapter four presents the development of the fringe projection system. The necessary parameters such as scaling factor, fringe projection angle were identified. In chapter five, an experimental work was carried out on six different spherical caps at different location inside the image field of view. The profile of the spherical cap was measured at different cross-sections. The root mean square errors of the spherical caps were calculated and the volume of each cap was calculated and compared to the actual one. The scanned shapes were modelled using STL file format to keep a permanent record of the shape. Chapter six describes a shape similarity method and an algorithm was applied to measure the similarity between the 3-D scanned shapes. Finally, chapter seven draws conclusions from the research described in this thesis and outlines areas for further research.

2.1 Introduction

Today, many non-contact measurement systems exist. These systems are used in different applications such as reverse engineering, where a CAD file is created for an existing physical part. These system have also been used in further applications beyond surface measurement, e.g. Avril et al. (2004) used Fourier fringe analysis to detect cracks in plates, Ratnam et al. (2001) used shadow moiré and neural network to classify eggs, Tan et al. (2000) combined a laser tracking technique and fringe projection method into one optical system to track objects, Spagnolo et al. (1997) measured the vibration amplitude of objects using fringe projection method and Fast Fourier Transform (FFT). Their work show that non-contact measurements can be engaged with other sciences for further developments. Within this chapter, it will be shown that the use of non-contact measurement to measure the tumour volume is a well-known application. The different non-contact measurements are also reviewed in this chapter (Section 2.2). This Section does not review non-contact measurement systems, but rather focuses on volume determination using non-contact techniques.

For the purpose of measuring the volume of object having a smooth surface using a non-contact system, it is necessary to use a segmentation method to extract the surface from the background. The literature in Section 2.3 describes different segmentation methods concerning the triangulated mesh of the known surface points.

After the shape is extracted from the background and its volume is determined, a record of the tumour volume and the 3-D shape can be kept inside a database. This database may contain the name, address, sex, age, medication and other details of the patient. A new facility can be added to help the clinicians to search for similar tumours or 3-D shape from inside this database. For example, the clinician might search for

similar 3-D shapes or skin disorders due to mosquito bites and access the offered medication. The term shape similarity is used to measure the similarity between shapes and is taking more attentions from scientists to develop new algorithms, as there is no definite definition for a 3-D shape. Section 2.3 reviews various publications in the area of shape similarity.

2.2 Volume Determination using Non-contact Devices

In the past, tumour volume measurement is not getting enough attention from researchers. There was more attention in two relevant subjects, wound and female breast volume measurement. This section presents different techniques and methods that define the volume of these three subjects.

Frankowski, et al. (2000 and 2002) proposed a commercial system called PRIMOS (Phaseshift Rapid In vivo Measurement Of Skin). This system is the closest to this research. The system is calibrated before measurement on steps, blocks, disks and grid. The system uses the digital micromirror devices (DMD) technology to project the fringe pattern three times on the human skin. A fourth image is captured to acquire the colours. All these images are captured in 64 ms. The system can calculate the volume of pores, scar, lesion and moles. A background subtraction is performed to eliminate the human skin data and leaving only the alimant. The limitations of this system are image noise and cost. The presence of noise in the image captured by the camera would lead to high errors in height, as three images are required to calculate the volume. The value of one system is more than 45,000 Euros (207,000 RM).

Boersma et al. (2000) developed a photogrammetry system consisting of three video cameras to determine the wound volume. The volume was defined as the region bounded between two surfaces: the measured surface of the wound and the original, healthy skin surface. In their research, the original healthy skin underneath the wound was created by cubic spline interpolation. The measured surface of the wound was

similar 3-D shapes of skin disorders due to mosquito bites and access the offered medication. The term shape similarity is used to measure the similarity between shapes and is taking more attentions from scientists to develop new algorithms, as there is no definite definition for a 3-D shape. Section 2.3 reviews various publications in the area of shape similarity.

2.2 Volume Determination using Non-contact Devices

In the past, tumour volume measurement is not getting enough attention from researchers. There was more attention in two relevant subjects, wound and female breast volume measurement. This section presents different techniques and methods that define the volume of these three subjects.

Frankowski, et al. (2000 and 2002) proposed a commercial system called PRIMOS (Phaseshift Rapid In vivo Measurement Of Skin). This system is the closest to this research. The system is calibrated before measurement on steps, blocks, disks and grid. The system uses the digital micromirror devices (DMD) technology to project the fringe pattern three times on the human skin. A fourth image is captured to acquire the colours. All these images are captured in 64 ms. The system can calculate the volume of pores, scar, lesion and moles. A background subtraction is performed to eliminate the human skin data and leaving only the alimnt. The limitations of this system are image noise and cost. The presence of noise in the image captured by the camera would lead to high errors in height, as three images are required to calculate the volume. The value of one system is more than 45,000 Euros (207,000 RM).

Boersma et al. (2000) developed a photogrammetry system consisting of three video cameras to determine the wound volume. The volume was defined as the region bounded between two surfaces: the measured surface of the wound and the original, healthy skin surface. In their research, the original healthy skin underneath the wound was created by cubic spline interpolation. The measured surface of the wound was

processed using a software called Softplotter and the volume was obtained using the program. Their experiment was performed on flat surface with texture and plastic models of different sizes of pressure sores. The limitation of this procedure is that training on the Softplotter software is necessary to the clinicians to calculate the volume.

Jones et al. (1995) introduced the prototype of the MAVIS (Measurement of Area and Volume Instrument System) based on a structured lighting method. The system consists of a projector and a CCD camera connected to a computer. An image is captured for the distorted stripes over the wound and the surrounding skin. Another image is captured for the wound without the projected stripe. The volume of the ulcer was defined as the region enclosed by the former healthy skin and the existing ulcer surface. In their research, the healthy skin was interpolated using the cubic spline, which performed better than Bezier curves. In order to calculate the volume, the rectangular surface grid (60 rows by 52 columns) is subdivided into a mesh of triangles. The volume was found by multiplying the area of a triangle by its average depth or height of the three vertices and summing over all triangles within the wound boundary. The disadvantage of this method is that taking the average of three height values does not guarantee accurate results in volume calculation.

Rogers et al. (1997) used a laser line generator for illumination and two video cameras for image acquisition. The laser and the cameras were mounted in a scanning head that moves on a linear track. An image is captured for the projected line and the head is moved to a new location where another image was captured. This process was repeated until the wound is completely scanned. Properties such as wound perimeter, area and volume can be obtained by host software. This software was developed by the authors under Microsoft Windows application using OpenGL. The (x, y, z) point data were interpolated and used to generate a regular grid of the wound. The healthy skin surface was approximated using spline. The system was tested on holes of known

geometry and simulated wounds on plaster models. Measurements were performed five times for each hole. The system has a disadvantage of long time scanning with no guarantee to keep the patient stand still for the whole measurement process.

Krouskop et al. (2002) projected a grid of points to measure the volume of wounds. The volume was defined as the region bounded between the original healthy skin and the measured surface. The original healthy skin was approximated using second order least square fitting. They noticed that the approximation method does not suite all body parts. The error in volume of the measurement system decreases by increasing the wound size.

Structure lighting method was also used for breast volume measurement of nursing mothers. Ng et al. (1994) used black face paint to mark the boundary of the breast. In the volume computation part, the two end points of each light stripe curve were used to determine the baseline of the chest wall. All the other 3-D points on the light stripe curve were then projected onto the baseline to get the height values. This procedure was done for each line stripe curve. Finally, adjacent light stripe curves gave the volume using the trapezoidal rule, i.e. summing up the small volumes of all the triangular prisms.

2.3 Segmentation Methods

Razdan et al. (2003) defined the word segmentation by breaking down an existing structure into meaningful, connected subcomponents. On the other hand, Benko et. al. (2004) stated that if the surface were known, one could collect all point being within a given threshold to that surface, and declare this set of points as the region belonging to the surface. Segmentation can be implemented using edge detection technique, region growing technique or a hybrid approach using edge detection and region growing (Razdan et al. 2003). The research work relevant to the

problem of 3-D object segmentation can be divided into three categories: (i) range data, (ii) 3-D point clouds and (iii) mesh.

In range data, the image of the scanned object is viewed as a piecewise smooth surface which is different than structured lighting method. Besl et al. (1988) defined eight types of surfaces (peak, flat, pit, minimal, ridge, saddle, valley, saddle valley) according to the sign of Gaussian and mean curvatures that were calculated using the neighbourhood points. Their method is based on variable order surface fitting (degree less than five). If the approximation is accepted, the fitting stops, otherwise the order of the polynomial is increased by one.

3-D point clouds are the known surface points of a scanned object. Figure 2.1 shows the known surface points of a flat object using a scanning device (e.g. laser scanning, structured lighting). Vanco et al. (2002) calculated the point normal vector and principal curvatures based on the neighbourhood information. Their segmentation method was performed in two steps. In the first step, sharp edges, regions of high curvature and flat areas in the object are detected using the point normal vectors. The angle between the point normal vectors of two adjacent points within one segment has to be smaller than angle α (defined by the user). The angle between the normal vector of a point and a reference vector has to be smaller than angle β (defined by the user). The reference vector of a segment is defined as the normalized sum of normal vectors of all points in the segment. In the second segmentation step, a segment is initialized using a single point and the neighbourhood points are included into the segment after satisfying the threshold values. The minimum and maximum of the first threshold values are the minimum and maximum deviation of the principal curvatures for two neighbourhood points. The minimum and maximum of the second threshold values are the average of the minimum and maximum principal curvature within the segment respectively. This segmentation method has a disadvantage that the calculation needs many parameters to set by the user.

Yang et al. (1999) used local parametric quadric surface approximation of the neighbourhood data points to estimate the local surface curvature. They were able to find surface boundaries using the extremes and zero crossing of curvature on a mesh. This segmentation is not suitable in noisy cloud data.

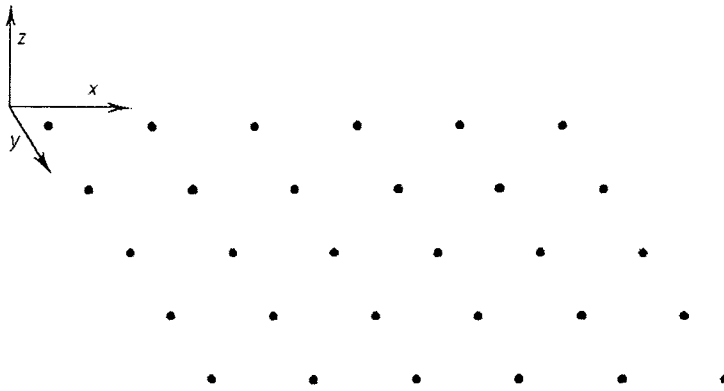


Figure 2.1: Known surface points of a flat object.

Lavoue et al. 2005 stated that only few published studies concern the problem of 3-D object segmentation using the 3-D triangulated surface mesh. The work in this area is necessary as triangulated surfaces are becoming one of the standard formats to model shapes and to exchange between different computers (e.g. STL files in CAD applications). An example of a triangular mesh is shown in Figure 2.2, where a set of known surface points are connected to neighbouring vertices by edges.

Mangan et al. (1999) generalized the watershed segmentation used in 2D image to 3-D triangular mesh. Their method is based on the curvature value of each vertex. A token move from one vertex to its neighbour until it reaches the minimum curvature and label is assigned to each minima. Each minima serves as the initial basis for a surface segment. All regions that have a watershed depth lower than the threshold are merged. The segmentation has a disadvantage of long computation time as the segmentation is repeated until all minimum curvatures are found.

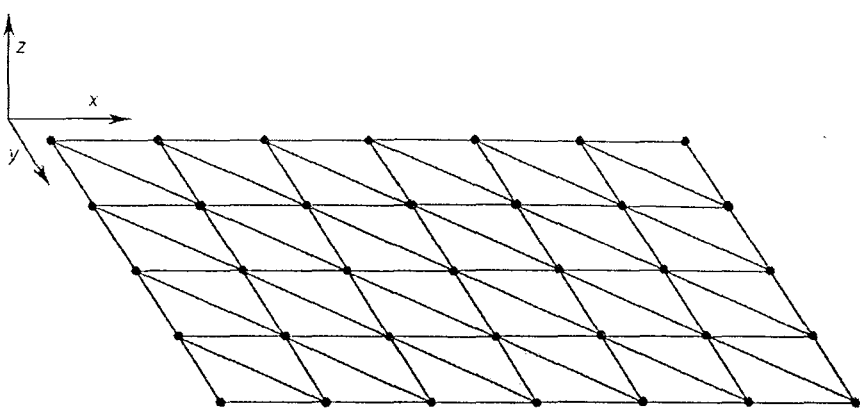


Figure 2.2: Example of a triangulated mesh of known surface points of a flat object.

Razdan et al. (2003) presented a hybrid approach segmentation. Their segmentation method combined the watershed segmentation developed by Mangan et al. (1999) and edge detection. An edge is detected if the normal vectors make an angle greater than a threshold angle (dihedral angle) between polygon faces.

Lavoue et al. (2005) presented a mesh segmentation based on the curvature tensor. Their approach is based on two steps. In the first step, the sharp edges and vertices are identified and the curvature tensor is calculated for each vertex. A region growing algorithm was applied to connect the vertices according to their principal curvature. In the second step, a boundary score computed using the curvature direction is used to mark the correct boundary edges coming from the region segmentation and followed by a contour tracking to obtain a set of closed contours.

Benko et al. (2004) used a direct segmentation based on discarding triangles in the vicinity of edges to divide the surface points into smaller, distinct point regions keeping G1 continuity (where the tangents to each curve at the point of connection have the same direction). The points were classified into either stable or unstable. The stable regions are kept so they can be approximated by a single surface. The classification was performed using tests that use indicators. The first indicator (geometric) uses the normal vector, principal curvature, best fit direction of linear

extrusion, or best fit axis of revolution. The second indicator (error) is based on normalised errors of least-squares fitting. The third test is based on similarity indicator and calculated in two phases. In the first phase, a geometric indicator is assigned to the point. In the second phase, the average sum of the magnitude of the difference vectors between the assigned geometric indicator vector of the current point and those in a neighbourhood is calculated. The point is considered stable, if the surrounding points have 'similar' indicator values to the current one. In order to define a threshold value to use for these indicators, four statistical tests were used. The first test is based on histograms of the error or scalar similarity indicator. The second test computes the standard deviation of the indicator in each neighbour point. In the third test, a point is considered stable if the indicators are approximately the same. The last test compares two full distributions computed from two neighbourhoods and decides the relative difference of the mean values and/or the standard deviation. The segmentation method is more suitable for CAD files that need extrusion or revolution features.

Pan et al. (2004) developed a segmentation algorithm using a flatness measure. The flatness measure was defined as a function of the triangle area and the normal. Firstly, the mesh is divided into different patches based on the flatness measure. The segmentation consists of three steps: (i) find the local minima and label the faces with different flags, (ii) find the initial patch sets and (iii) merge patches using a local to global strategy.

Park et al. (2002) proposed an automated segmentation for reverse engineering application. The triangle mesh is generated from the input data point and aggregated into a region until the area of the region reaches a user-defined area criterion. The boundaries are detected by comparing the triangle normal to the user defined angle criteria. These boundaries are inputs for a neural network to extract six features from the surface. These features are pocket, step, boss, slot, hole and block. Their segmentation method is limited to mechanical features.

Woo et al. (2002) studied the application of octree-based method in 3-D segmentation. Their work is similar to the work developed in this research. A triangular mesh is generated for the measured points. For each vertex the normal values of each surrounding triangle is considered. The triangle normal is calculated for each surrounding triangle (n_i in Figure 2.3) and the average of these normal is assigned to the vertex (N in Figure 2.3). The algorithm starts with an initial 3-D grid that encloses the object. The standard deviation of the point normal direction with respect to one of the three axes (x, y, z) and the surrounding vertices is the criteria used to divide the initial grid. If the standard deviation is higher than the user specification, the grid is divided into eight daughters. The disadvantage of this segmentation method is that the segmentation results will change by setting different normal direction in (x, y, z).

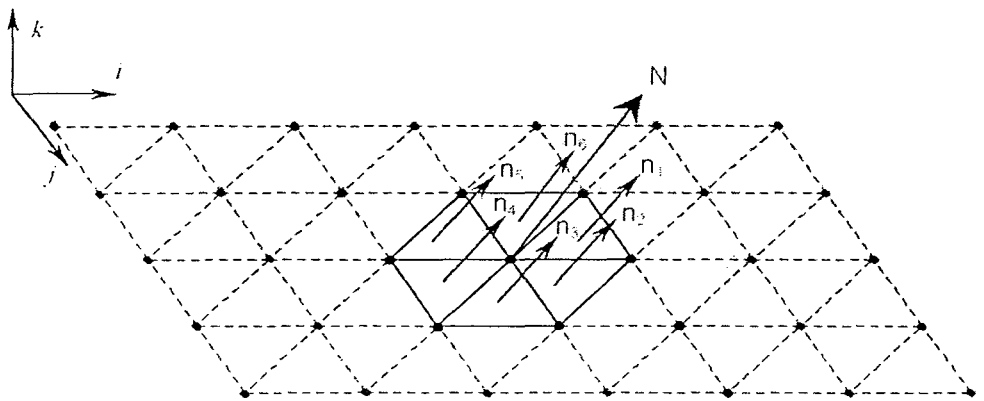


Figure 2.3: Schematic of point normal calculation of the method proposed by H. Woo et al. (2002)

2.4 Shape Similarity

Skin disorders scanned using the developed structured lighting method can be presented in a 3-D shape. Clinicians can use these 3-D shapes for diagnosis, monitoring and retrieval. Traditionally, these shapes can be stored into a database and textual information is assigned to each shape. The advantage of textual indexing of 3-D shape is that it can provide clinicians with keyword searching. The limitation is that it consumes much time when the database is large in size or when the database without

textual information is exported or imported. As a result, there has been a new focus on developing 3-D shape indexing called 3-D shape similarity. Researchers achieved the shape similarity between 3-D models in the database using the following three steps:

- 1- Analysis of the geometry
- 2- Shape description
- 3- Similarity measure

Analysis of the geometry is performed to define a standard position for the 3-D object. Using this position allows different algorithms to perform the model translation, rotation and scaling invariance. The next step is shape description where the shape is transformed into a descriptor. The similarity measure is used to answer the question how much similar is the query shape to the remaining 3-D objects in the database. This step uses the distance similarity (or dissimilarity) function where the lower the dissimilarity measure the higher the similarity between these two 3-D object.

Several measures were used for the distance similarity between two sets of features $H = \{h_i\}$ and $K = \{k_j\}$, where h_i and k_j are the feature element. The most used measure in 3-D shape is element-by-element dissimilarity measures. One of these measures is the *Minkowsky-form distance* function and defined by Butos et al. (2004) as follows:

$$L_p(H, K) = \left(\sum_i |h_i - k_i|^p \right)^{1/p} \quad (2.1)$$

where L is the dissimilarity value and p is an integer value. For the case where $p = 1$, the Minkowsky distance is called the Manhattan or City-block distance and has an abbreviation l_1 , while the Minkowsky distance with $p = 2$ is called the Euclidean distance and has an abbreviation l_2 . In this research, the Euclidean distance was used

for dissimilarity measure. Figure 2.4 shows the comparison which is done between corresponding element h_i and k_j , at only $i=j$.

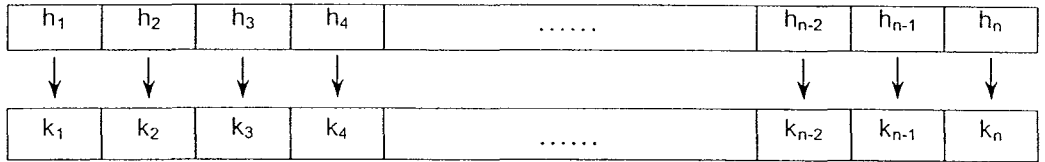


Figure 2.4: Element-by-element similarity measure

Authors in the past have used different techniques to describe a 3-D shape, which can be divided into three different methods: Feature based method, Histogram based method and Topology based method

2.4.1 Feature-based Method

This method is based on extracting features from the 3-D shape that describe the descriptor. The similarity measure is performed between these descriptors.

2.4.1.1 Statistical Approach

Osada et al. (2001 & 2002) proposed a statistical approach named the shape distribution, where a certain number of points on the 3-D object surface are chosen. Five geometric properties (shape function) were developed in their work:

- A_3 measures the angle between three random points on the surface of a 3-D model.
- D_1 measures the distance between the centroid of the boundary of the model and one random point on the surface.
- D_2 measures the distance between two random points on the surface.
- D_3 measures the square root of the area of the triangle between three random points on the surface.

- $D4$ measures the cubic root of the volume of the tetrahedron between four random points on the surface.

Among these five shape functions, the $D2$ measure shows the most effective results in shape similarity applied on 133 models divided into 25 classes, such as: planes, phones, pens, mugs, tanks, boats, sofas...etc.

2.4.1.2 Moments

Paquet et al. (2000) decomposed the outer surface of the 3-D shape into a triangular mesh and proposed the moments based-descriptor based on statistical moment. The moment was calculated using the following equation (Paquet et al. 2000):

$$M_{qrs} = \sum_{i=1}^n S_i (x_i - x_{CM})^q (y_i - y_{CM})^r (z_i - z_{CM})^s \quad (2.2)$$

where, x_i , y_i and z_i are the co-ordinate of the centre of mass of the i^{th} triangle, n is the total number of triangles that constitutes the object surface, x_{CM} , y_{CM} and z_{CM} are the coordinates of the centre of mass of the object, S_i is the mass of the i^{th} triangle and the sum $q+r+s$ is the order of the moment.

2.4.1.3 Geometric Parameters

Geometric features such as area, volume, surface area and bounding box have been used to describe the shape. Zhang et al. (2001a and 2001b) extracted features such as volume, area, volume-surface ratio and aspect ratio from the model. The Euclidean distance was used to measure the similarity between two models. The disadvantage of these features that models having same volume or area are considered similar although they might be different in shape.

Ohbuchi et al. (2002) divided the model into l equal thickness slabs along each of the principal axes and used the statistics values of three statistics along each of the

three principal axes: (i) the moment of inertia about the axis, (ii) the average distance to surfaces from that axis, and (iii) the variance of distance to surfaces from the axis. The similarity distance between features was calculated using the Euclidean distance. There was no specific slab number for each model. The change in slab number of each model leads to a change in results.

Paquet et al. (2000) defined the bounding box of the model and used properties such as (i) the fractional occupancy (ratio of the object volume to the volume of its bounding box), (ii) depth, height and width of the bounding box and (iii) bounding box centroid. Each property is used separately according to the user demand. The disadvantage of their work that the rotation and translation invariance were not secured. Their work is similar to the work developed in this research.

Corney et al. (2002) used 101 L-shape blocks and proposed three properties. The first property is the hull crumpliness (ratio of the object's surface area to the surface area of its convex-hull), the second property is the hull packing (percent of the convex hull volume not occupied by the original object) and the last property is the hull compactness (ratio of the convex hull's surface area cubed over the volume of the convex hull squared). Their work is limited to the use of L-shape blocks.

2.4.2 Histogram-based Method

Paquet et al. (1999) proposed the cords-based method. The outer object surface is composed of a triangular mesh and a cord is then defined as a vector that connects the model centre of gravity and the centroid of each triangle. This chord produced three histograms. The first histogram represents the distribution of the angles between the cords and the first principle axis of the shape, while the second histogram provides the distribution of the angles between the cords and the second principle axis

of the shape. The third histogram describes the distribution of the chord length. If the chord length is taken as it is, the histogram is scale dependent. While normalizing the chord length values between zero for the shortest chord and one for the longest chord make this histogram scale independent.

Liu et al. (2003) proposed the Directional Histogram Model (DHM). A number of sampling directions are defined and the thickness of the model at different cross sections is obtained. The histogram is represented by a 3-D function to define the direction and thickness value. This method can not be used for scanned models where the model is a surface without a thickness.

2.4.3 Topology-based Method

The topology method is based on the description of the model topology. The 3-D shape is converted into a graph using skeleton-like presentation. The descriptor is the graph and the dissimilarity measure is performed between these two graphs. Hilaga et al. (2001) proposed the Multi-resolution Reeb Graph (MRG). In this case, a continuous function was applied to each vertex of the surface model (assuming a triangular decomposition of the model surface). This function is the integration of the geodesic distance between two vertices. At this point, the Reeb Graph is constructed by dividing the model into a number of levels based on the value of the scalar function. Each level is presented by a node, and connected to the adjacent node by an edge. The disadvantage of this method is that surfaces with one patch are always similar as their graph is always one node.

2.5 Summary

Although different non-contact measurement systems were used to calculate the volume of moles, wound, nursing female breast, etc, authors agreed that the volume is the region sandwiched between two surfaces. The first surface is the original healthy skin and the second surface is measured surface (tumour). Different published work showed better results when the original healthy skin is approximated using spline interpolation. The method of calculating the volume by dividing the projected area into triangles and the total volume is the summation of all prisms shows an error less than 10%. This calculation method does not guarantee that the shape of the calculated volume is the same as the shape of the measured tumour.

The different segmentation methods developed by the authors needs the calculation of neighbourhood information such as Gaussian, mean, principal curvature and normal values. These parameters would be difficult to clinicians (or other staff working in the medicine area) to understand and handle. A segmentation based on simple algorithm has to be developed to suite the application.

In shape similarity, three steps are needed to measure the similarity distance between 3-D shapes. The first step is to define a reference position. In the second step, a set of features is extracted from the 3-D shape to form a descriptor. While similarity distance between models in the last step is calculated by the Minkowsky function or an equivalent function. It is important to extract features that are understood by normal users. This makes it easy to measure the similarity between a model in mind that does not exist in the database and all models in the database. These features are physical quantity such as volume, surface area, height, width or depth. Other features need an experienced user to estimate the feature values.

CHAPTER THREE
A SIMULATION STUDY ON THE EFFECT OF FRINGE SPACING ON
DIFFERENT VOLUME CALCULATION METHODS
IN STRUCTURED LIGHTING

3.1 Introduction

One of the methods to determine the 3-D coordinates on a surface with minimum error is by using structured lighting. Structure lighting technique involves projecting patterns of light upon a surface of interest and capturing an image of the resulting pattern as reflected by the surface. The image must then be analyzed to determine the 3-D coordinates of data points on the surface (Varady, et al, 1997). Figure 3.1 shows the principle of a structured lighting method. A grating (normally placed inside a projector) is used to illuminate the object with the projected pattern. The pattern has definite fringe or line spacing. The grating is inclined at a predefined angle θ relative to the camera. The camera is placed above the object and able to capture an image of the surface with the projected pattern. A part of the projected pattern hits the surface and part of it continues on the flat background. Most structured lighting methods use triangulation equation to obtain the height values of the scanned surface.

The sketch in Figure 3.2 shows the image of the scanned surface in Figure 3.1 as seen by the camera. This simulated image shows the top view of the surface with the projected pattern. The lines of the projected pattern surrounding the object surface are straight. This happens due to the flat background in which the object was placed. The falling pattern lines on the surface are distorted according to the surface profile. The x , y , z data along these lines can be known and defined, while elsewhere are unknown as the projected lines does not exist. The aim of this part of the work is to calculate the volume of a certain shape using these known data.

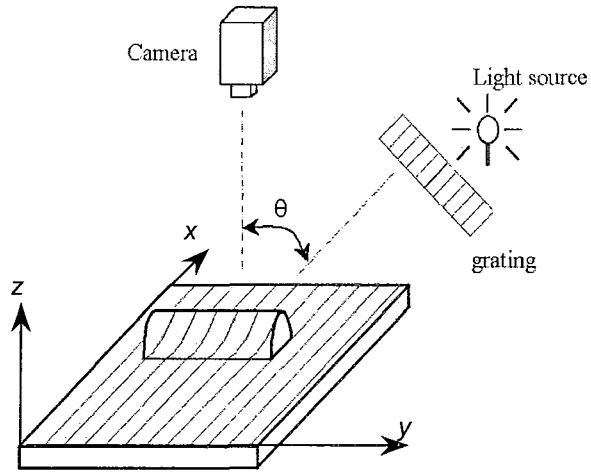


Figure 3.1: Structured lighting principles

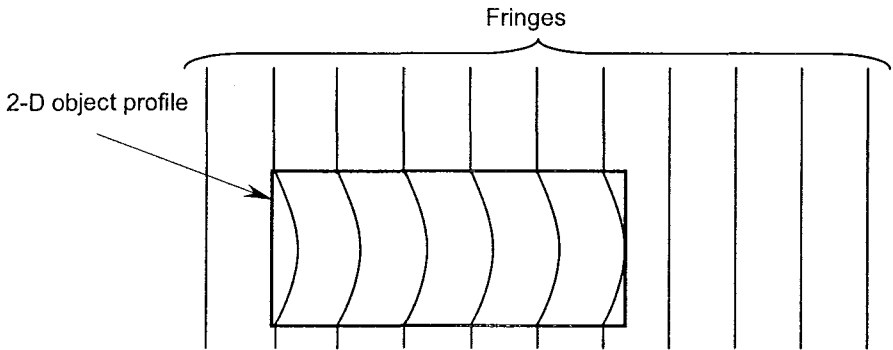


Figure 3.2: Sketch of the captured image for the scanned object in Figure 3.1

3.2. Volume Calculation

In order to determine the volume of a skin disorder two surfaces have to be known: the measured surface of the disorder and the original healthy skin surface (Boersma et al. 2000). The volume is defined as the region bounded between both surfaces and could be computed using the multiplication of area of base by height

method or integration of a fitted curve across coordinate points and multiplied by its depth along x-direction.

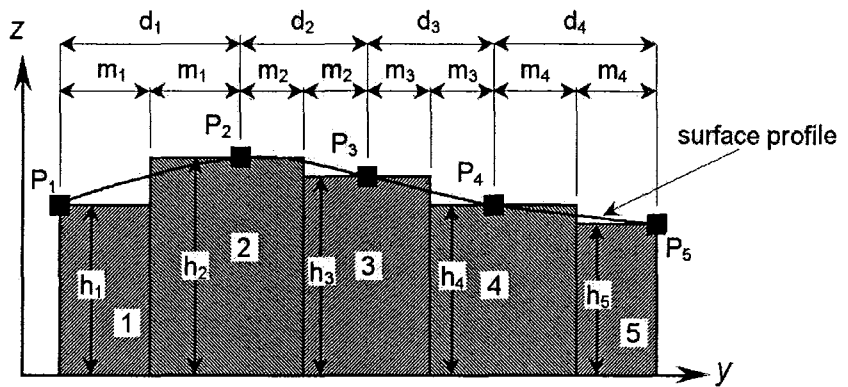
3.2.1 Volume Determination using Multiplication of Area of Base by Height Method

In this method, the measured shape is divided into a number of smaller shapes and the projected area of each of the smaller shape is calculated. The volume is obtained by multiplying each projected area (base) by the height. In this research, the base was a rectangle. The rectangle width equals to one pixel, the smallest integer units of an image. The length of the shape is divided into many rectangle lengths for approximation. Figure 3.3(a) shows a schematic example of volume calculation at a certain surface x-section. The surface points measured by a structured lighting technique are presented by squares. The distances between known surface points are known and assigned by the dimension d_i . In this example, the first and last known surface points are assumed to be the limits of the measured profile. Otherwise, a segmentation method followed by an extrapolation is necessary to obtain these two points. The area under the profile is divided into five shapes and assigned by an integer number. Each shape encloses one known surface point. Figure 3.3(b) shows the different shape of rectangles each with a depth equal to w . The rectangle's length l is defined under three conditions:

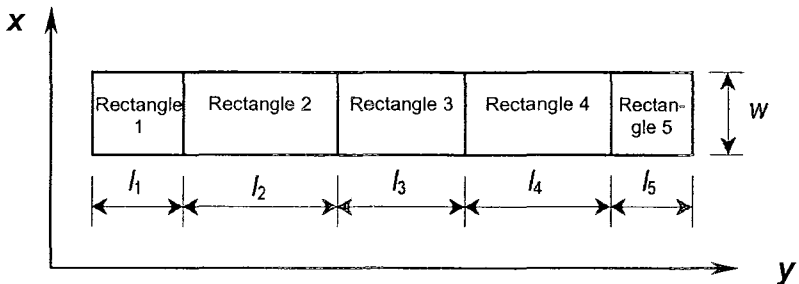
- (i) The left limit of the measured profile. The length is the half distance between a known height point and its next one in the same x-section.
- (ii) The right limit of the measured profile. The length is the half distance between a known height point and its previous one in the same x-section.
- (iii) Otherwise, the length is the summation of two distances. The first distance is the half distance between a known height point and its next one in the same x-

section. The second distance is the half distance between a known height point and its previous one in the same x-section.

These three conditions define the length of the *rectangle_i* in Figure 3.3(b) as follows: $l_1 = m_1$, $l_2 = m_1 + m_2$, $l_3 = m_2 + m_3$, $l_4 = m_3 + m_4$, $l_5 = m_4$. The area of each *rectangle_i* is multiplied by the height h_i . Each h_i value in the figure equals to the height of the enclosed coordinate. Finally, the total volume is the volume summation of these rectangle-based shapes.



(a)



(b)

Figure 3.3: Schematic of volume calculation using area of base times height (a) The division of area under the measured surface profile (b) Top view of the created rectangles.

3.2.2 Volume Determination using Curve Fitting

The volume is calculated by a method similar to the previous one. Instead of dividing the area under the measured data points, a fitted curve is used to interpolate or approximate the surface profile. The integration of the curve determines the area under the profile. The multiplication of the area under the curve by the depth along x -direction gives the volume.

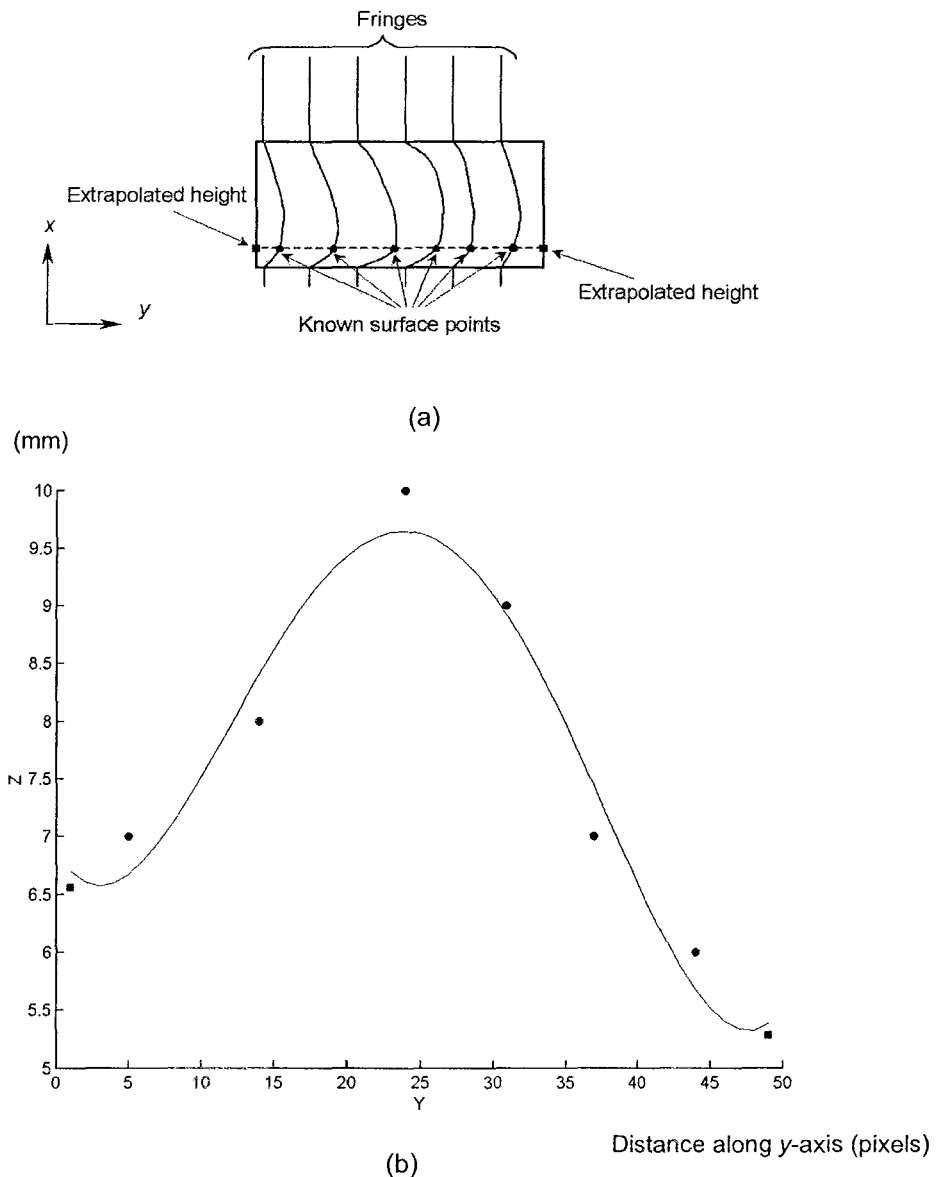


Figure 3.4: Plan and front views for known surface points. (a) Plan view for the surface and the direction of fitted curve. (b) Front view.